Dynamic Cooperativity of Chromophores in Promoting Singlet Fission in Perylenediimide Crystal

Lijuan Xue, Haibei Huang, Yuxiang Bu*

School of Chemistry and Chemical Engineering, Shandong University, Jinan 250100, People's Republic of China

Contents

1. Excited State Energies and Frontier Molecular Orbital Energies of the PDI Monomer

Table S1. Excited state energies and frontier molecular orbital Energies of the optimized ground state structure of the PDI monomer (static and gaseous).

	S_1 (eV)	T_1 (eV)	ΔE_{SF} (eV)	HOMO energy (eV)	LUMO energy (eV)	H-L GAP (eV)
B3LYP	2.370	1.220	0.070	-6.455	-3.971	2.484
PBE0	2.460	1.241	0.022	-6.628	-3.862	2.766
M062X	2.834	1.638	0.442	-7.433	-3.081	4.352

Note: $\Delta E_{SF} = 2 \times E(T_1) - E(S_1)$ and all were calculated at the 6-31+G (d, p) level.

2. Dynamic Simulation Data of PDI Crystal Extracted PDI Fission Cluster

Scheme S1. Local excitation for each monomer PDI(A), PDI(B), PDI(C) or PDI(D) in crystal found at different times, respectively.
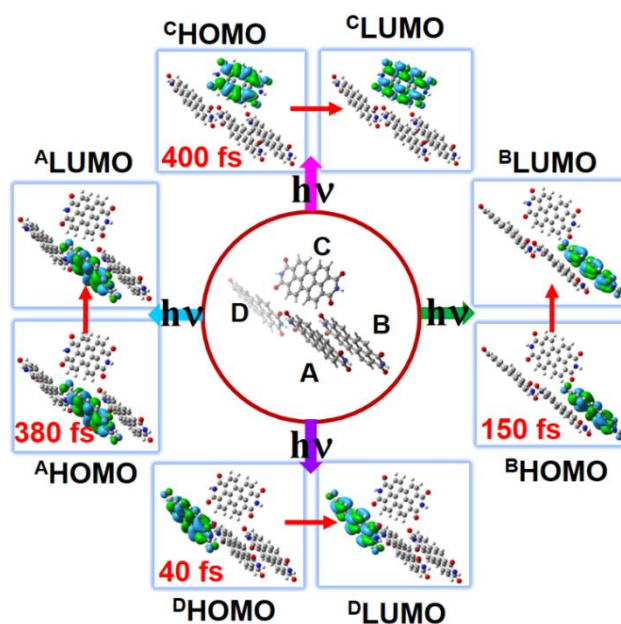
Table S2. The example of electron transitions of excited states and their corresponding frontier molecular orbitals for PDI fission cluster when PDI (A) is excited.

Time/fs	Excited states	Energy (eV)	Transition Configuration	Orbital transition	ΔE_{SF}
	S_{1A}	2.274	$397 \rightarrow 402$ 0.62507 ^{A}HOMO $\rightarrow$ ^{A}LUMO (78.1%)	$\rightarrow$	
	T_{1A}	1.069	$397 \rightarrow 402$ 0.63214 ^{A}HOMO $\rightarrow$ ^{A}LUMO (79.9%)	$\rightarrow$	-0.218 **PDI(A)-PDI(B)**
75 fs	T_{1B}	0.987	$398 \rightarrow 401$ 0.66030 ^{B}HOMO $\rightarrow$ ^{B}LUMO (87.2%)	$\rightarrow$	-0.277 **PDI(A)-PDI(C)**
	T_{1C}	0.928	$399 \rightarrow 403$ 0.68000 ^{C}HOMO $\rightarrow$ ^{C}LUMO (92.5%)	$\rightarrow$	-0.291 **PDI(A)-PDI(D)**
	T_{1D}	0.914	$400 \rightarrow 404$ 0.71468 ^{D}HOMO $\rightarrow$ ^{D}LUMO (100%)	$\rightarrow$	
	S_{1A}	2.297	$397 \rightarrow 402$ 0.67838 ^{A}HOMO $\rightarrow$ ^{A}LUMO (92.0%)	$\rightarrow$	
	T_{1A}	1.156	$397 \rightarrow 402$ 0.68026 ^{A}HOMO $\rightarrow$ ^{A}LUMO (92.6%)	$\rightarrow$	-0.278 **PDI(A)-PDI(B)**
140 fs	T_{1B}	0.863	$398 \rightarrow 401$ 0.70989 ^{B}HOMO $\rightarrow$ ^{B}LUMO (100%)	$\rightarrow$	0.105 **PDI(A)-PDI(C)**
	T_{1C}	1.246	$399 \rightarrow 404$ 0.68977 ^{C}HOMO $\rightarrow$ ^{C}LUMO (95.2%)	$\rightarrow$	-0.175 **PDI(A)-PDI(D)**
	T_{1D}	0.966	$400 \rightarrow 403$ 0.71265 ^{D}HOMO $\rightarrow$ ^{D}LUMO (100%)	$\rightarrow$	

Time/fs	Excited states	Energy (eV)	Transition Configuration	Orbital transition	ΔE_{SF}
	S_{1A}	2.308	397 → 401 0.58624 ^{A}HOMO → ^{A}LUMO (68.7%)		
	T_{1A}	1.234	397 → 401 0.69416 ^{A}HOMO → ^{A}LUMO (96.4%)		0.008 **PDI(A)-PDI(B)**
320 fs	T_{1B}	1.082	398 → 402 0.70389 ^{B}HOMO → ^{B}LUMO (99.0%)		0.351 **PDI(A)-PDI(C)**
	T_{1C}	1.425	400 → 404 0.69025 ^{C}HOMO → ^{C}LUMO (95.3%)		0.199 **PDI(A)-PDI(D)**
	T_{1D}	1.273	399 → 403 0.69982 ^{D}HOMO → ^{D}LUMO (97.9%)		
	S_{1A}	2.241	397 → 401 0.59594 ^{A}HOMO → ^{A}LUMO (71.0%)		
	T_{1A}	1.060	397 → 401 0.69226 ^{A}HOMO → ^{A}LUMO (95.8%)		-0.138 **PDI(A)-PDI(B)**
650 fs	T_{1B}	1.043	398 → 402 0.67287 ^{B}HOMO → ^{B}LUMO (90.6%)		0.213 **PDI(A)-PDI(C)**
	T_{1C}	1.394	399 → 404 0.67133 ^{C}HOMO → ^{C}LUMO (90.1%)		0.011 **PDI(A)-PDI(D)**
	T_{1D}	1.192	400 → 403 0.70219 ^{D}HOMO → ^{D}LUMO (98.6%)		

Table S3. The example of electron transitions of excited states and their corresponding frontier molecular orbitals for PDI fission cluster when PDI (B) is excited.
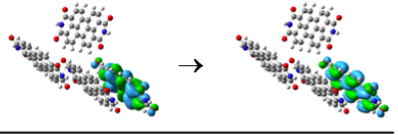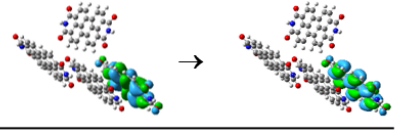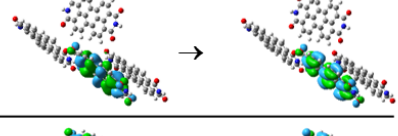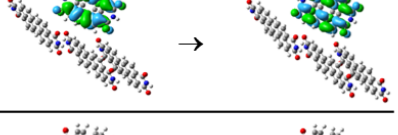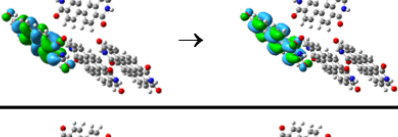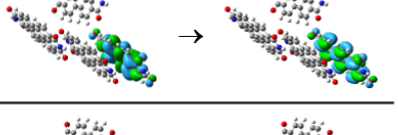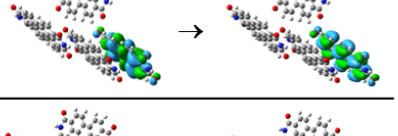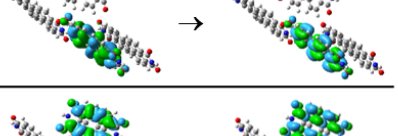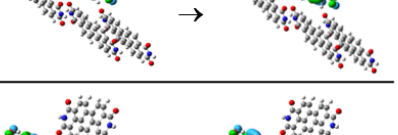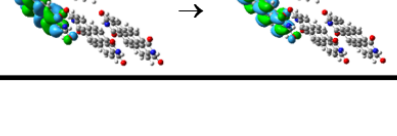
Time/fs	Excited states	Energy (eV)	Transition Configuration	Orbital transition	ΔE_{SF}
	S_{1B}	2.332	$398 \rightarrow 402 \quad 0.65810$ $^{B}HOMO \rightarrow {}^{B}LUMO$ (86.6%)	$\rightarrow$	
	T_{1B}	1.215	$398 \rightarrow 402 \quad 0.69848$ $^{B}HOMO \rightarrow {}^{B}LUMO$ (97.6%)	$\rightarrow$	-0.053 **PDI(B)-PDI(A)**
390 fs	T_{1A}	1.064	$397 \rightarrow 401 \quad 0.69816$ $^{A}HOMO \rightarrow {}^{A}LUMO$ (97.5%)	$\rightarrow$	0.166 **PDI(B)-PDI(C)**
	T_{1C}	1.283	$399 \rightarrow 403 \quad 0.68179$ $^{C}HOMO \rightarrow {}^{C}LUMO$ (92.9%)	$\rightarrow$	0.163 **PDI(B)-PDI(D)**
	T_{1D}	1.280	$400 \rightarrow 404 \quad 0.68825$ $^{D}HOMO \rightarrow {}^{D}LUMO$ (94.7%)	$\rightarrow$	
	S_{1B}	2.325	$397 \rightarrow 402 \quad 0.50534$ $^{B}HOMO \rightarrow {}^{B}LUMO$ (73.3%)	$\rightarrow$	
	T_{1B}	1.196	$397 \rightarrow 402 \quad 0.56884$ $^{B}HOMO \rightarrow {}^{B}LUMO$ (64.7%)	$\rightarrow$	-0.329 **PDI(B)-PDI(A)**
430 fs	T_{1A}	0.800	$398 \rightarrow 401 \quad 0.64452$ $^{A}HOMO \rightarrow {}^{A}LUMO$ (83.1%)	$\rightarrow$	-0.182 **PDI(B)-PDI(C)**
	T_{1C}	0.947	$400 \rightarrow 403 \quad 0.67766$ $^{C}HOMO \rightarrow {}^{C}LUMO$ (91.8%)	$\rightarrow$	0.132 **PDI(B)-PDI(D)**
	T_{1D}	1.261	$399 \rightarrow 404 \quad 0.6900$ $^{D}HOMO \rightarrow {}^{D}LUMO$ (95.2%)	$\rightarrow$	

Table S4. The example of electron transitions of excited states and their corresponding frontier molecular orbitals for PDI fission cluster when PDI (C) is excited.

Time/fs	Excited states	Energy (eV)	Transition Configuration	Orbital transition	ΔE_{SF}
	S_{1C}	2.329	$400 \to 404$ 0.62159 ^{C}HOMO $\to$ ^{C}LUMO (77.3%)	$\to$	
	T_{1C}	1.210	$400 \to 404$ 0.68372 ^{C}HOMO $\to$ ^{C}LUMO (93.5%)	$\to$	-0.014 **PDI(C)-PDI(A)**
160 fs	T_{1A}	1.105	$397 \to 401$ 0.66513 ^{A}HOMO $\to$ ^{A}LUMO (88.5%)	$\to$	0.170 **PDI(C)-PDI(B)**
	T_{1B}	1.289	$398 \to 402$ 0.66912 ^{B}HOMO $\to$ ^{B}LUMO (89.5%)	$\to$	0.129 **PDI(C)-PDI(D)**
	T_{1D}	1.248	$399 \to 403$ 0.69847 ^{D}HOMO $\to$ ^{D}LUMO (97.6%)	$\to$	
	S_{1C}	2.229	$400 \to 404$ 0.59440 ^{C}HOMO $\to$ ^{C}LUMO (70.6%)	$\to$	
	T_{1C}	1.056	$398 \to 403$ 0.65564 ^{C}HOMO $\to$ ^{C}LUMO (86.0%)	$\to$	0.074 **PDI(C)-PDI(A)**
520 fs	T_{1A}	1.247	$397 \to 402$ 0.66174 ^{A}HOMO $\to$ ^{A}LUMO (87.6%)	$\to$	-0.078 **PDI(C)-PDI(B)**
	T_{1B}	1.095	$398 \to 403$ 0.65564 ^{B}HOMO $\to$ ^{B}LUMO (85.9%)	$\to$	-0.288 **PDI(C)-PDI(D)**
	T_{1D}	0.885	$399 \to 401$ 0.71307 ^{D}HOMO $\to$ ^{D}LUMO (100%)	$\to$	

Table S5. The example of electron transitions of excited states and their corresponding frontier molecular orbitals for PDI fission cluster when PDI (D) is excited.

Time/fs	Excited states	Energy (eV)	Transition Configuration	Orbital transition	ΔE_{SF}
410 fs	S_{1D}	2.105	$400 \to 404$ 0.64127 $^{D}HOMO \to {}^{D}LUMO$ (82.2%)	$\to$	
	T_{1D}	1.045	$400 \to 04$ 0.72097 $^{D}HOMO \to {}^{D}LUMO$ (100%)	$\to$	-0.209 **PDI(D)-PDI(A)**
	T_{1A}	0.851	$397 \to 401$ 0.61146 $^{A}HOMO \to {}^{A}LUMO$ (74.8%)	$\to$	-0.070 **PDI(D)-PDI(B)**
	T_{1B}	0.990	$398 \to 402$ 0.57297 $^{B}HOMO \to {}^{B}LUMO$ (665.7%)	$\to$	-0.181 **PDI(D)-PDI(C)**
	T_{1C}	0.879	$399 \to 403$ 0.66076 $^{C}HOMO \to {}^{C}LUMO$ (87.3%)	$\to$	
500 fs	S_{1D}	2.243	$400 \to 404$ 0.6659 $^{D}HOMO \to {}^{D}LUMO$ (88.7%)	$\to$	
	T_{1D}	1.112	$400 \to 404$ 0.70437 $^{D}HOMO \to {}^{D}LUMO$ (99.2%)	$\to$	-0.039 **PDI(D)-PDI(A)**
	T_{1A}	1.092	$397 \to 401$ 0.60964 $^{A}HOMO \to {}^{A}LUMO$ (74.3%)	$\to$	-0.032 **PDI(D)-PDI(B)**
	T_{1B}	1.099	$398 \to 402$ 0.62104 $^{B}HOMO \to {}^{B}LUMO$ (77.1%)	$\to$	0.025 **PDI(D)-PDI(C)**
	T_{1C}	1.156	$399 \to 403$ 0.69871 $^{C}HOMO \to {}^{C}LUMO$ (97.6%)	$\to$	

Table S6 (a). The example of singlet excitation energy $E(S_1)$ and oscillator strength f when PDI (A) is excited at 380 fs.

380 fs excited	Energy	Oscillator strength
S_{1A}	2.277	1.4904
$\textbf{S}_{\textbf{1B}}$	1.976	0.015
S_{1C}	2.201	0.5740
S_{1D}	2.181	0.0174

Table S6 (b). The example of singlet excitation energy $E(S_1)$ and oscillator strength f when PDI (B) is excited at 150 fs.

150 fs excited	Energy	Oscillator strength
S_{1A}	2.303	0.3857
S_{1B}	2.446	0.9722
S_{1C}	2.408	0.2655
S_{1D}	2.258	0.5911

Table S6 (c). The example of singlet excitation energy $E(S_1)$ and oscillator strength f when PDI (C) is excited at 400 fs.

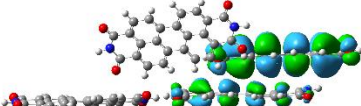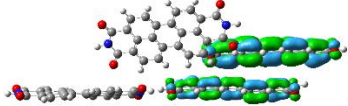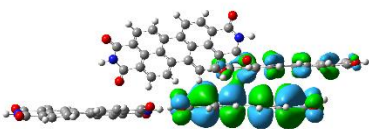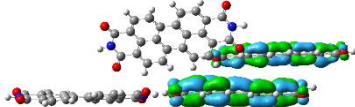| 400 fs Excited	Energy	Oscillator Strength
S_{1A}	2.068	0.1921
S_{1B}	1.958	0.0053
S_{1C}	2.214	1.0244
S_{1D}	2.352	0.0459
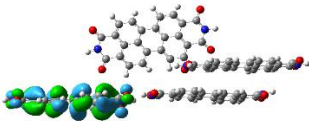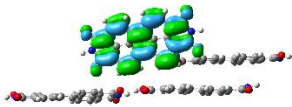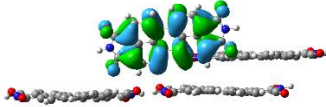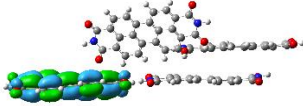
Table S6 (d). The example of singlet excitation energy $E(S_1)$ and oscillator strength f when PDI (D) is excited at 40 fs.

40 fs Excited	Energy	Oscillator Strength
S_{1A}	2.433	0.7953
S_{1B}	2.156	0.3132
S_{1C}	2.356	0.2771
S_{1D}	2.231	1.056

Table S7. The example of singlet excitation energy $E(S_1)$ and triplet excitation energy $E(T_1)$ when ε has different values.

ε	T_{1A} / eV	S_{1A} / eV	T_{1B} / eV	S_{1B} / eV
5.00	1.2118	2.2187	1.2390	2.2761
6.30	1.2130	2.2184	1.2395	2.2753
7.50	1.2132	2.2183	1.2396	2.2752

Table S8. The HOMO and LUMO Distributions of PDI cluster.

	Frontier Molecular Orbital		Frontier Molecular Orbital
HOMO		LUMO+3	
HOMO-1		LUMO+2	
HOMO-2		LUMO+1	
HOMO-3		LUMO	

We recheck the layout of exciton wave functions of the transient configurations, and it is found that the exciton wavefunctions of the majority of transient configurations are localized to individual PDI units, and a few configurations are not localized on individual units, as shown in Table S8.
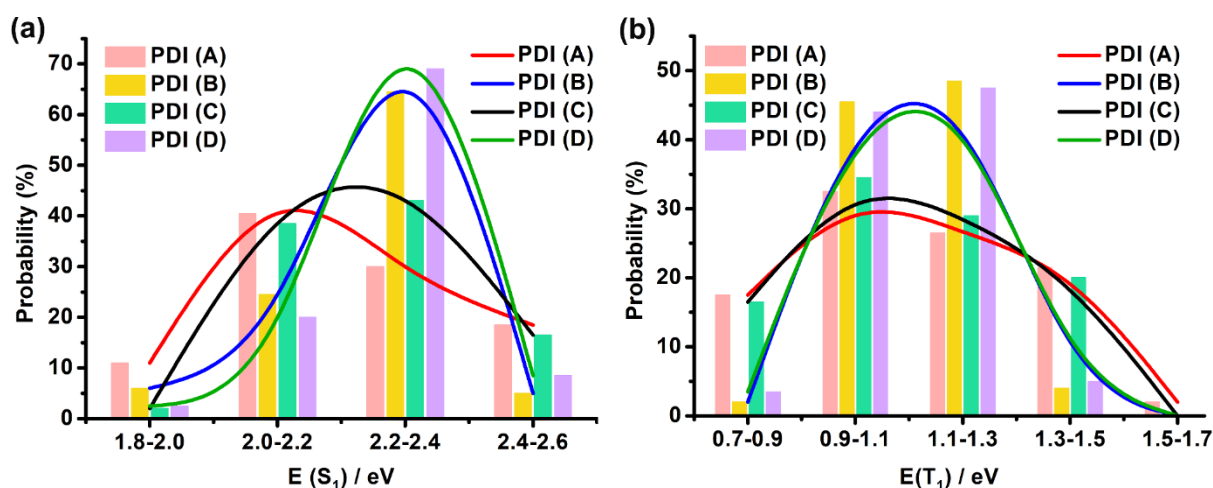
Figure S1. (**a**) The probabilities of excitation energy intervals of the singlet state (E(S$_1$)) for 200 transient configurations of PDI (A), PDI (B), PDI (C) and PDI (D) in a 1 ps AIMD trajectory. The red, blue, black and green fitting curves are associated with the light pink, orange, light-green, violet columns, respectively. (**b**) The probabilities of excitation energy intervals of the corresponding triplet states (E(T$_1$)) for these 200 transient configurations of PDI (A), PDI (B), PDI (C) and PDI (D). The red, blue, black and green fitting curves are associated with the light pink, orange, light-green, violet columns, respectively.

To research the SF between the central-excited monomer and the adjacent monomers of PDI during the distortion of dynamic geometric, AIMD simulation was performed on the PDI crystal (Scheme 1c) for 5 ps, and we extract the 200 transient geometries from a 1 ps window in the 5 ps trajectory of PDI (A) centered fission clusters (Scheme 1d) in the cell. First of all, the excitation energy distribution of all chromophores is determined according to the calculated E(S$_1$) and E(T$_1$), and the localization cases of excited states of all the transient geometries for every PDI SF cluster. E(S$_1$) and E(T$_1$) for every monomer change with time during the distortion of dynamic geometric. The configuration of each monomer PDI (A), PDI (B), PDI (C) or PDI (D) of the PDI SF cluster changes constantly with time, which leads to the periodic change of singlet and triplet excitation energies of each PDI monomer with the change of transient configuration. For the PDI monomers, E(S$_{1A}$), E(S$_{1B}$), E(S$_{1C}$) and E(S$_{1D}$) change in a range of 1.84-2.60 eV, 1.81-2.46 eV, 1.89-2.55 eV, 2.00-2.48 eV with a large fluctuation and the maximum distribution for E(S$_{1A}$), E(S$_{1B}$), E(S$_{1C}$) and E(S$_{1D}$) are at 2.00-2.40 eV, 2.20-2.40 eV, 2.00-2.40 eV and 2.20-2.40 eV (Figure S1a). E(T$_{1A}$), E(T$_{1B}$), E(T$_{1C}$) and E(T$_{1D}$) change in the

between of 0.70-1.60 eV, 0.86-1.38 eV, 0.72-1.49 eV, and 0.73-1.39 eV with also large fluctuations, and the maximum distributions for $E(T_{1A})$, $E(T_{1B})$, $E(T_{1C})$ and $E(T_{1D})$ are all at 0.90-1.30 eV (Figure S1b). The dynamic structure disturbance causes a certain difference between every monomer in the crystal of the excited energies ($E(S_1)$, $E(T_1)$), but the difference is slight. Due to the influence of intermolecular arrangement and intermolecular vibration, the excited energy of each monomer oscillates with time, making the singlet and triplet excited energy oscillate about 1.81-2.60 eV and 0.70-1.60 eV, respectively, which inevitably affect the excited-transformation of exciton between the PDI excited monomer and its adjacent PDI monomers.
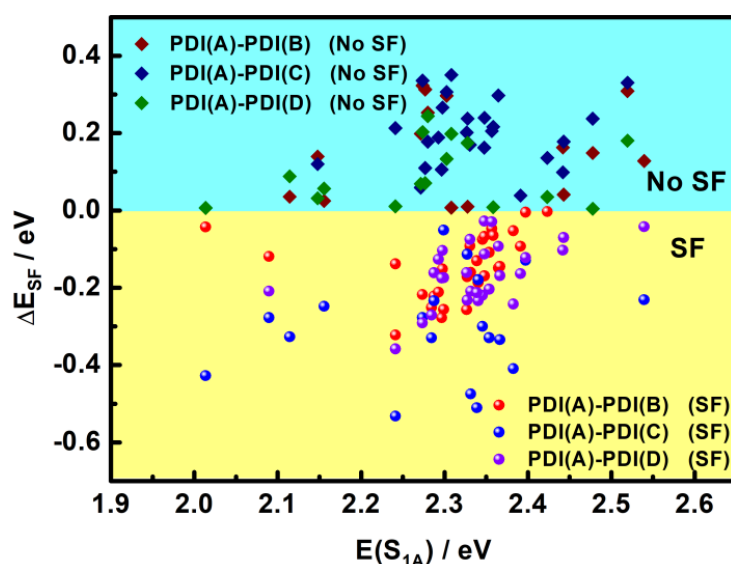

Figure S2 (A). The correlation between ΔE_{SF} and $E(S_1)$ of the PDI fission cluster for some transient configurations extracted from a 1 ps time window in the AIMD simulation trajectory when PDI(A) is excited, respectively. The yellow areas denote $\Delta E_{SF} \leq 0$, SF undergoing.
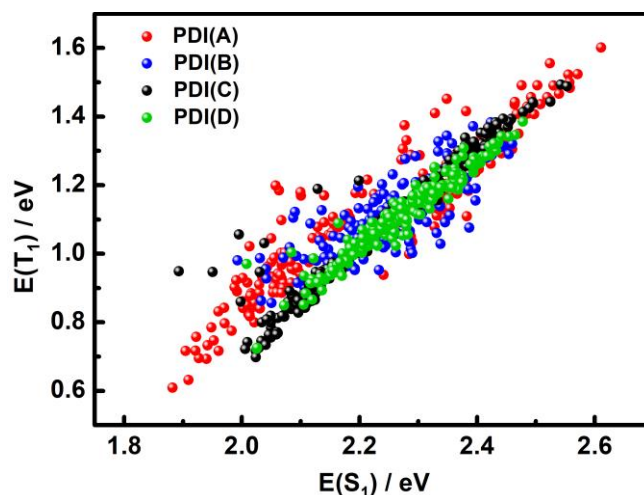
Figure S2 (B). The correlation between $E(T_1)$ and $E(S_1)$ of PDI(A), PDI(B), PDI(C) and PDI(D) for 200 transient geometries.

We also investigate the correlation between $E (S_1)$ and $E (T_1)$ of PDI monomers, and Figure S2 (B) displays the correlations of $E(S_1)$ with $E(T_1)$ of PDI(A), PDI(B), PDI(C) and PDI(D) for 200 transient geometries. As shown in Figure S2 (B), there is a nicely linear correlation between the S_1 and T_1 exciton energies for individual PDI monomer.

3. Dynamic Simulation Data of Electronic Couplings for PDI Dimer
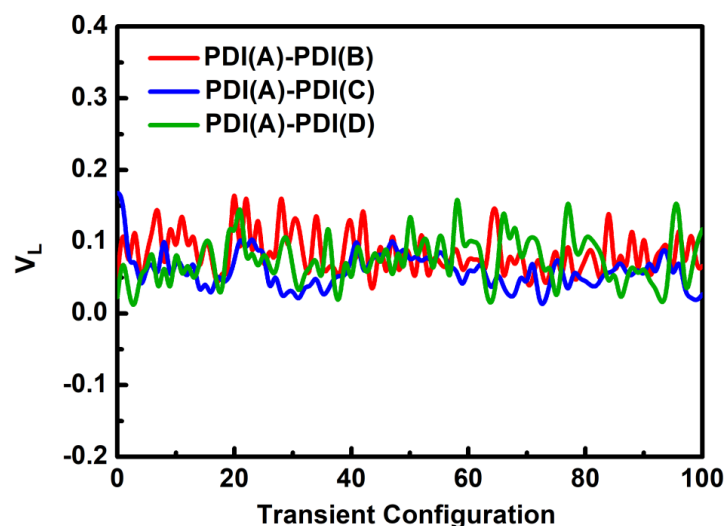

Figure S3. Electronic coupling (V_L, eV) for electron transfer of the PDI(A)-PDI(B), PDI(A)-PDI(C) and PDI(A)-PDI(D) quasi-dimers for 100 transient geometries extracted in which PDI (A) is excited. V_L denotes their LUMO coupling.

The electronic coupling matrix elements for electron transport V_L of the PDI(A)-PDI(B), PDI(A)-PDI(C), PDI(A)-PDI(D) quasi-dimers for 100 transient configurations in which PDI (A)-centered is excited are calculated, respectively. As illustrated in Figure S1, the electron transport V_L for the PDI(A)-PDI(B), PDI(A)-PDI(C) and PDI(A)-PDI(D) quasi-dimers change with time, but they are not significantly different.
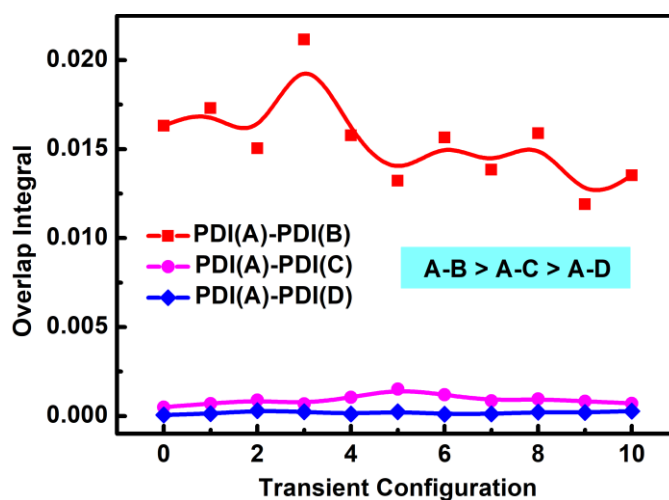

Figure S4. The HOMO-LUMO overlap integrals of the PDI(A)-PDI(B), PDI(A)-PDI(C) and PDI(A)-PDI(D) quasi-dimers in 10 transient configurations of the PDI cluster extracted from the AIMD simulation trajectory in which PDI (A) is excited.

According to the Michl work (Smith, M. B.; Michl, J. Recent Advances in Singlet Fission. *Annu. Rev. Phys. Chem.* **2013,** *64*, 361-386 and Havlas, Z.; Michl, J. Guidance for Mutual Disposition of Chromophores for Singlet Fission. *Isr. J. Chem.* **2016**, 56, 96-106, *DOI: 10.1002/ijch.201500054*), the SF rate can be simplified as a relation with the overlap integral between two associated monomers (i.e. the electronic coupling is determined by the simple structure-dependent factor, the overlap integral). Thus, to verify the electronic coupling between different dimers, we calculate the HOMO(A)-LUMO(X) (X=B, C, D) overlap integral of PDI dimers, which can reflect the actual status of the HOMO(A)→LUMO(X) electron transfer transition in SF. The calculated results are shown in Figure S4, indicating that the overlap integral of PDI(A)-PDI(B) is the largest, followed by the PDI(A)-PDI(C) pair, and the PDI(A)-PDI(D) pair is the smallest. This indirectly indicates the existence of electronic

coupling between two proximate PDI, and the PID(A)-PDI(B) pair has the strongest electronic coupling and can undergo SF.

4. Dynamic Simulation Data of the Structure for PDIs
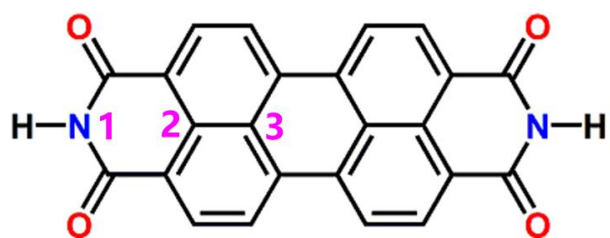
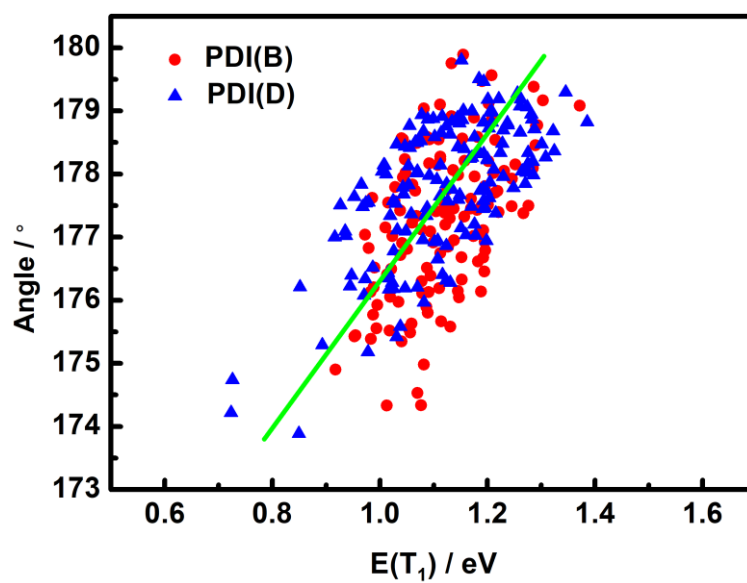**Scheme S2.** A schematic structure of a PDI monomer in the static geometry.

Figure S5. Correlation between the angle $\angle$N1-C2-C3 and E(T$_1$) of PDI(B) and PDI(D).
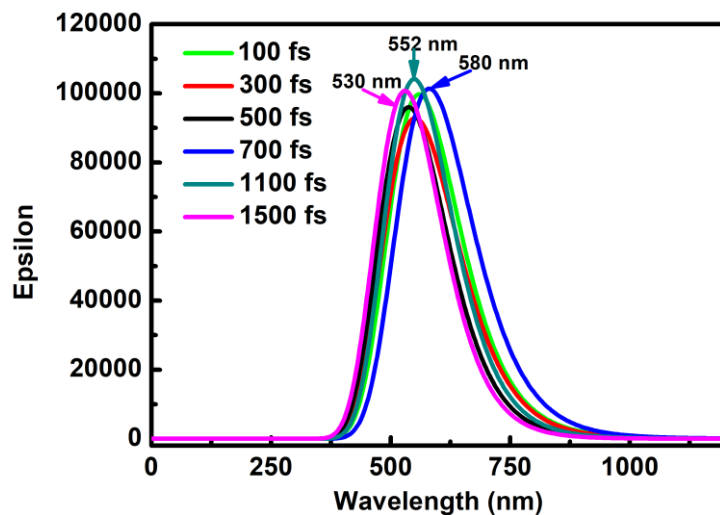
Figure S6. The calculated UV−vis absorption spectra of the PDI clusters extracted from the AIMD simulation trajectory.
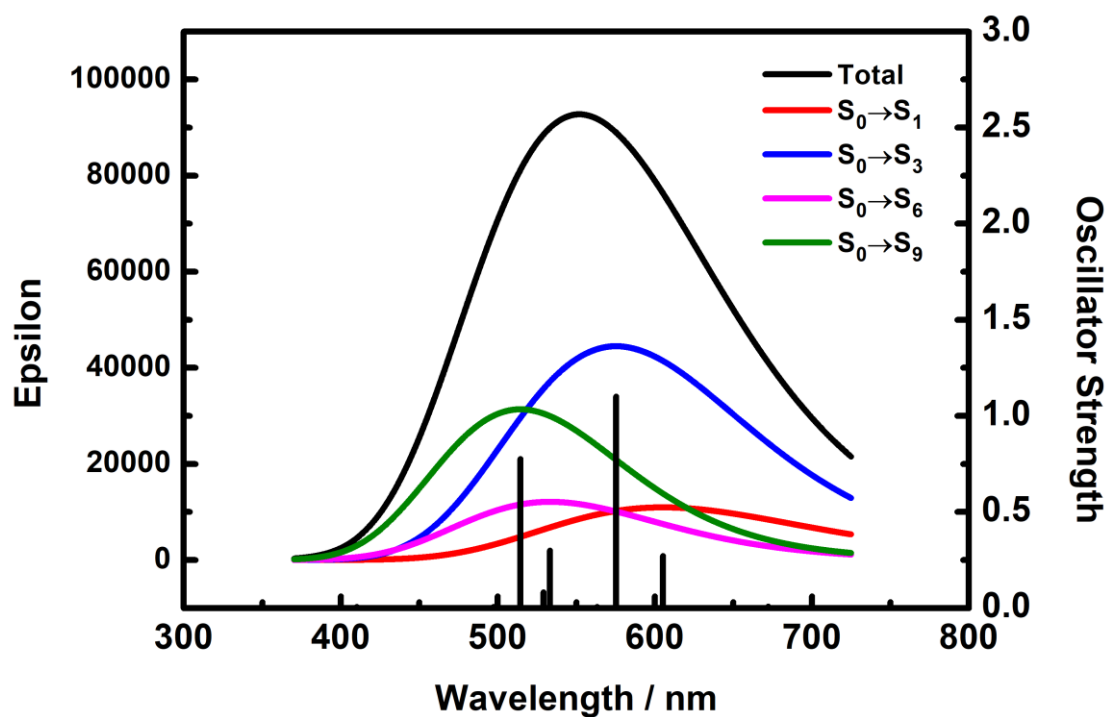

Figure S7. The calculated UV−vis absorption spectrum and transition modes with oscillator strengths greater than 0.1 of the PDI clusters extracted from the AIMD simulation trajectory at 300 fs.

We calculated UV-vis absorption spectrum (**Figure S6**), but the spectrum in **Figure S6** actually is the sum of 20 excited states not only for the S_1 state.　To clarify the components of this UV-vis absorption spectrum, **Figure S7** shows the total UV-vis spectrum and transition modes with oscillator strengths greater than 0.1 (i.e., decomposition of the total spectrum) at 300 fs.　The peak of the overall absorption curve often corresponds to a transition with greater intensity.　However, due to all transitions contributing to the absorption curve of the nearby range, the position of the peak does not always correspond to the energy of the transition with higher intensity, whether it is the actual spectrum or the theoretically simulated spectrum.　For example, in the above figure, the oscillator strength of $S_0{\rightarrow}S_3$ is 1.1001, and that of $S_0{\rightarrow}S_9$ is 0.7754.　In addition, there are the transitions $S_0{\rightarrow}S_6$ (oscillator strength of 0.2991) and $S_0{\rightarrow}S_1$ (oscillator strength of 0.2706), and their contributions to the spectrum (shown by the red and magenta curves) are much smaller than that of $S_0{\rightarrow}S_3$ (shown by the blue curve, the main transition).　In short, they all contribute to the overall spectrum, resulting in the breadth of the spectrum as shown in **Figure S6**.

Currently, many approximations are used in all theoretical methods, and the calculated vertical excitation energy and the maximum peak of the absorption spectrum do not strictly correspond to each other.　Therefore, there inevitably are differences between the experimental and theoretical results.　As long as the calculated and experimental results are within a specific error range, and the approximate range of the principal peak is consistent, the theoretically calculated results could be considered to be reasonable and reliable and can be used for analyses on this basis.